Chinese Chemical Letters 35 (2024) 109296

Contents lists available at ScienceDirect

Chinese Chemical Letters

journal homepage: www.elsevier.com/locate/cclet

Gold mineralized "hybrid nanozyme bomb" for NIR-II triggered tumor effective permeation and cocktail therapy

Ji Liu[a,1], Dongsheng He[a,1], Tianjiao Hao[a,1], Yumin Hu[b], Yan Zhao[c], Zhen Li[a], Chang Liu[a], Daquan Chen[d,*], Qiyue Wang[e,*], Xiaofei Xin[a,*], Yan Shen[a,*]

[a] Department of Pharmaceutics, State Key Laboratory of Nature Medicines, China Pharmaceutical University, Nanjing 210009, China
[b] Wuxi Hequan Pharmaceutical Co., Ltd., Wuxi 214029, China
[c] Beijing Xinghao Yingsheng Pharmaceutical Co., Ltd., Beijing 102609, China
[d] School of Pharmacy, Yantai University, Yantai 264005, China
[e] School of Pharmaceutical Science, Nanjing Tech University, Nanjing 211816, China

ARTICLE INFO

Article history:
Received 4 September 2023
Revised 5 November 2023
Accepted 8 November 2023
Available online 11 November 2023

Keywords:
Gold mineralized
Hybrid nanozyme bomb
Starvation therapy
Cocktail therapy
NSCLC

ABSTRACT

Lung cancer is one of the most common malignant tumors with the fastest increase in the incidence rate and mortality. Even after maximum tumor resection assistance with a radiotherapy and chemotherapy combination, the recurrence of non-small cell lung cancer is still inevitable. In addition, low targeting efficiency and poor permeability of drug delivery systems strongly affect the therapeutic efficiency of anti-cancer drugs on non-small cell lung cancer. Here we designed a gemcitabine (GEM) loaded arginine-glycine-aspartic acid-cysteine (RGDc)-modified gold mineralization "hybrid nanozyme bomb" (RGTG) to overcome those obstacles. RGDc modification improved the active targeting of liposomes to the tumor tissues with the second near-infrared (NIR-II)-triggered gold-shell disruption and GEM release. The collapsed gold-shell particles with a smaller size could penetrate the tumor solid barrier and act as photothermal therapy (PTT) agents to improve PTT therapy and starvation therapy *via* generating gluconic acid and reactive oxygen species (ROS). Moreover, the resting reversal effect of gold particles on tumor fibroblasts can achieve accelerating tumor penetration of gold particles and GEM. Compared to monotherapy, RGTG showed significant improvement in tumor inhibition, with a tumor volume reduction of 83% compared to the control group, which provides a promising tumor treatment platform for non-small cell lung cancer (NSCLC).

Lung cancer has been considered the major cause of cancer mortality in adults [1]. Around 80%–85% of lung cancer patients were diagnosed with non-small cell lung cancer (NSCLC) with an overall 5-year survival rate of 59% and 25% of them face tumor relapse [2–4]. For the advanced NSCLC or patients unsuitable for surgery, combination therapeutic strategies urgently need to be developed to improve the NSCLC therapeutic efficiency due to the monotherapy resistance and poor efficiency. The metabolism of cells abnormally improved is one of the major physiological characteristics of cancers [5]. Therefore, tumor starvation therapy has been considered an effective method for inhibiting tumor cell proliferation by blocking their angiogenesis or inhibiting the supply of nutrition [6–9]. Moreover, starvation therapy could reduce the level of adenosine triphosphate (ATP) and induce down-regulation of heat shock protein levels in the tumor microenvironment, which also benefits hyperthermia therapy and increase synergistic tumor inhibition efficiency. Although the advantages have been reported for tumor therapy for several years, some key concerns such as low targeting efficiency, elevated tumor hypoxia, and increased tumor metastasis risk still are the obstacles that limited their application in cancer therapy [10,11].

Biomineralization is a process in which inorganic elements are specifically deposited on an organic substrate to form hard tissue materials [12–15]. Based on the mechanism of this natural biomineralization process, versatile nanoplatforms have been developed for a variety of biomedical applications [16,17]. Nanozymes are nanomaterials provided with intrinsic enzyme-like properties with the advantages of storage stability, economy, and convenient functional modification compared to natural enzymes [18,19]. It was reported that citrate-coated gold nanoparticles (GNPs) exhibited a glucose oxidase (GOx)-mimicking activity for the catalytic oxida-

* Corresponding authors.
E-mail addresses: cdq1981@126.com (D. Chen), qiyue.wang@njtech.edu.cn (Q. Wang), xxin@cpu.edu.cn (X. Xin), shenyan@cpu.edu.cn (Y. Shen).
[1] These authors contributed equally to this work.

https://doi.org/10.1016/j.cclet.2023.109296
1001-8417/

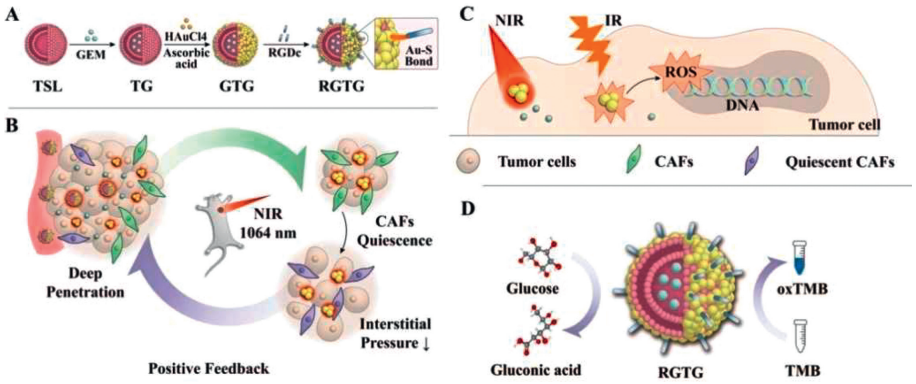

Scheme 1. Illustration of preparation steps of RGTG and its antitumor mechanism. (A) The preparation of targeting RGTG. (B) Penetration promoting mechanism. (C, D) Starvation therapy and cocktail therapy of RGTG.

tion of glucose with oxygen. Based on plenty of research, gold-based nanoparticles could exhibit the following key roles in tumor therapy [20]: (1) improve the consumption of glucose as an alternative strategy for cancer-starvation therapy; (2) improve the consumption of oxygen increases tumor hypoxia, which can be harnessed for hypoxia-activated therapy; (3) induce the generation of gluconic acid followed by enhances the acidity of the tumor microenvironment, which can trigger pH-responsive drug release; (4) induce the generation of H_2O_2 which increased the levels of reactive oxygen species (ROS) and tumor cell apoptosis after exposing to light irradiation or *via* Fenton reaction; (5) act as vaccine nanoadjuvants by promoting local inflammation to fight viral infections and tumors [21]; (6) improve the accuracy of cancer diagnosis, to avoid false-positive occur [22,23]. Therefore, the gold-based nanoparticle was applied as a muti-functional tumor therapy agent and to be investigated in different tumor therapy strategies [24]. In addition, inorganic nanomaterials can induce mitochondrial dysfunction by altering Ca^{2+} signaling channels in cancer cells, thereby damaging mitochondria and leading to cell apoptosis [25,26]. However, similar to nanocarriers, single metal mineralized nanozymes exhibited poor target permeability after administration and metabolic difficulties *in vivo*, which seriously affects their therapeutic efficiency of tumor starvation therapy alone or synergistic effects combined with other therapies. Surface modification of GNPs can significantly improve drug delivery efficiency and tumor targeting ability [27]. Arginine-glycine-aspartic acid-cysteine peptide (RGDc) can enhance the tumor targeting ability of gold nanoparticles by cross-linking them on the surface through Au-S bonds.

Therefore, we proposed a gemcitabine (GEM)-loaded gold mineralized hybrid nanozymes for tumor effective penetration and NSCLC treatment. The GEM-loaded temperature-responsive liposomes were prepared and then mineralized by gold on the surface followed by decoration of RGDc (Scheme 1A). RGDc-based active targeting contributes to the formulation accumulated in the tumor area. The tumor-located type II NIR irradiation was converted into heat due to the mineralized gold surface as photothermal therapy (PTT) agents and induced the liposome burst and release the GEM for tumor chemotherapy. The outside gold shells were collapsed with the liposomes and the left gold particles with a much smaller particle size could improve their tumor penetration in the solid area (Scheme 1B) and act as PTT sensitizer to improve PTT therapy and starvation therapy *via* gluconic acid and ROS generation (Schemes 1C and D). Moreover, the resting reversal effect of gold particles on tumor fibroblasts can achieve accelerating tumor penetration of gold particles and GEM. The gold-mineralized hybrid nanozymes could overcome the obstacles of poor tumor penetration and improve the synergistic effect of tumor chemotherapy, photothermal therapy, and starvation therapy, suggesting a promising tumor treatment platform for NSCLC.

In this work, we designed an RGDc modified gold mineralization "hybrid nanozyme bomb" (RGTG) for effective tumor penetration and NSCLC treatment. As shown in Figs. S1A and B (Supporting information), thermalsensitive liposomes (TSL) and gemcitabine hydrochloride loaded thermalsensitive liposomes (TG) were both spherical particles. The particle size of gold mineralized thermosensitive liposome (GTG) has increased to 141.42 ± 1.35 nm with a rough surface, which indicates that chloroauric acid was reduced to form a gold shell outside the liposomes. The particle size of RGTG has increased to 148.77 ± 1.79 nm with a similar morphology and particle size, suggesting the RGDc coating has no effects on the particle size (Figs. 1A and B). The zeta potential of formulations was also characterized. The TG exhibited a negative surface charge with the zeta potential of -28.47 ± 3.07 mV, while that of GTG and RGTG was 8.02 ± 0.32 and 6.47 ± 3.07 mV, respectively, suggesting the neutral gold shell coated outside the liposomes, which shielded the surface charges of liposomes (Fig. S1C in Supporting information) [28].

The encapsulation efficiency and drug loading of GEM in TG were 67.82% ± 4.55% and 8.64% ± 0.68%, respectively. The gold shell coating and RGDc modification had no impact on drug encapsulation and slightly decreased drug loading (70.24% ± 3.42% *vs.* 65.37% ± 7.53% for encapsulation efficiency; 6.69% ± 0.76% *vs.* 6.31% ± 0.56% for drug loading) (Figs. S1D and E in Supporting information). This might be due to the modification of RGDc and gold shell coating increasing the weight of the liposome, while the quality of the drug did not change significantly, resulting in a decrease in drug loading. In addition, we confirmed the RGDc grafting ratio was 12.73% by the bicinchoninic acid (BCA) method.

Ultraviolet spectroscopy and energy dispersive spectrometer (EDS) mapping further validated the successful construction of the gold mineralized "hybrid nanobomb" structure (Fig. 1C, Fig. S1F in Supporting information).

The results of photothermal conversion efficiency indicate that the modification of RGDc does not affect the photothermal conversion rate of GT, and RGTG exhibits stable photothermal conversion efficiency and limited attenuation (Figs. S3A–H in Supporting information).

Photothermal-response drug release behavior of RGTG triggered by the second near-infrared (NIR-II) laser was investigated under different pH conditions *in vitro* (Figs. S2, S3I and J in Supporting information). At pH 7.4, the free GEM was completely released within 6 h with a cumulative release of over 85%. The release of GTG and RGTG in the absence of NIR-II stimulation was similar to that of TG with sustained release effects. After NIR-II trigged, the cumulative drug release rate reached 68.17% and 65.91% after 24 h,

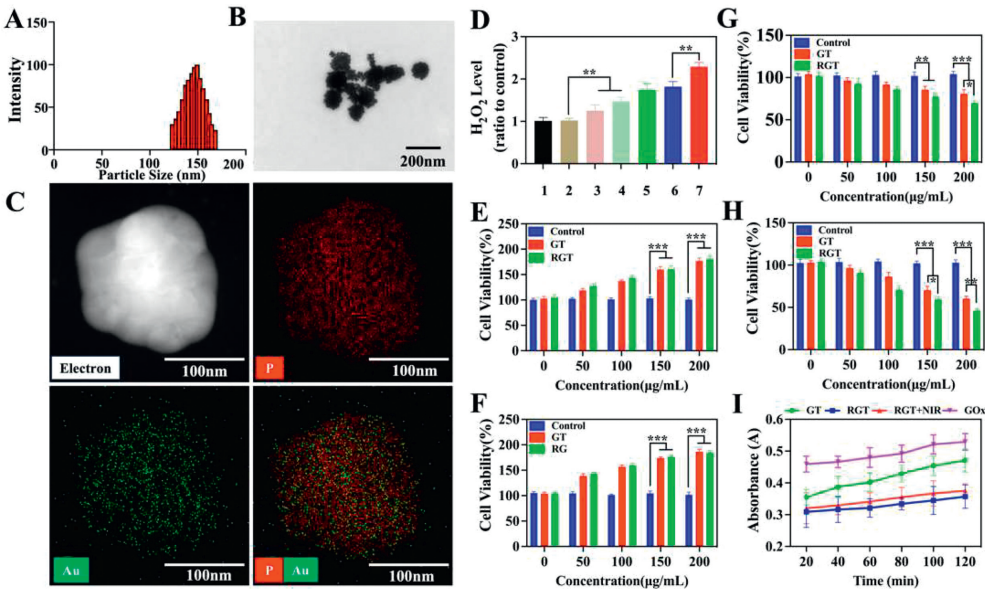

Fig. 1. The particle size (A) and transmission electron microscope (TEM) images (B) of RGTG (n=3). Scale bar: 200 nm. (C) The EDS mapping of RGTG. Scale bar: 100 nm. (D) H_2O_2 level was catalyzed by different formulations. 1: Control; 2: TSL; 3: GTG; 4: RGTG; 5: RGTG + NIR; 6: RGTG + IR; 7: RGTG + NIR + IR. (E–H) Cell viability without glucose at 24 h (E) and 48 h (F). Cell viability containing glucose at 24 h (G) and 48 h (H). (I) Results of catalytic activity of glucose like oxidase. Each bar represents the mean ± standard deviation (SD), n=3. $^{*}P < 0.05$, $^{**}P < 0.01$, $^{***}P < 0.001$.

which was significantly different from that of the group without NIR-II stimulation ($P < 0.01$), this may be due to the change in thermosensitive liposome membrane fluidity as well as permeability caused by temperature increase under NIR-II stimulation which leads to the drug release improvement. Compared with pH 7.4, the cumulative release of free GEM was higher at pH 5.4, reaching 92.82% at 4 h which is due to the high solubility of GEM in an acidic environment. The cumulative release of GTG and RGTG group was further increased ($P < 0.05$) to 65.38% and 67.29% after NIR-II irradiation, respectively, indicating that RGTG expressed an excellent NIR-II responsive drug release behavior and was more rapidly to release drugs under acidic conditions.

It has been reported that GNPs could catalyze the conversion of glucose to gluconic acid and hydrogen peroxide which reduced the pH of tumor sites and generate oxygen under the action of catalase [29]. Compared to TSL, the level of H_2O_2 produced by GTG and RGTG was significantly increased ($P < 0.01$). After RGDc modification, the amount of RGDc-modified gold mineralized thermal sensitive liposomes (RGT) entering the cell interior increased, and the level of H_2O_2 further increased compared to other groups. In addition, it was obvious that RGTG produced the most H_2O_2 after combined ionizing radiation (IR) and NIR irradiation ($P < 0.01$) (Fig. 1D).

GOx-induced glucose depletion has become the most used strategy for cancer starvation therapy. Glucose-fueled cell survival tests showed that the addition of GT and RGT to the medium without glucose significantly increased cell survival ($P < 0.001$) in a concentration-dependent manner. This might be due to liposomes providing nutrients and gold nanoparticles lacking substrates to produce ROS killer cells (Figs. 1E and F). Figs. 1G and H showed that GNPs catalyzed glucose in the medium to produce ROS killer cells in the presence of oxygen after the addition of glucose. Compared with the control group, cell viability was significantly decreased in GT and RGT groups ($P < 0.001$). After RGDc modification, catalyze efficiency could be far more improved due to the RGDc-based improvement of cellular uptake, in which the cell viability decreased significantly compared to GT ($P < 0.01$). Moreover, the 3,3′,5,5′-tetramethylbenzidine (TMB) method was used to evaluate the glucose oxidase-like activity of RGTG. Fig. 1I showed that the glucose oxidase-like activity of GT and RGT was time-dependent. Compared with GT, the absorbance of the RGT group decreased significantly during the same period, indicating that the catalytic ability of RGT was reduced, which may be due to the surface modification masking the active site of the enzyme and reducing its catalytic ability [30]. However, the catalytic ability of RGT was improved under the stimulation of NIR, which might be due to the loose structure of RGT and the increased exposure of active sites after NIR stimulation, enhancing its catalytic ability.

Gold nanoparticles have been reported to act as a sensitizer to reduce the irradiation dose in tumor therapy, thus reducing the damage to normal tissue caused by radiotherapy. IR can induce various types of DNA damage such as directly breaking the DNA chains by the deposited energy or indirectly through ROS produced by the radioactive decomposition of water molecules in cells [31,32]. GNPs can generate hydroxyl radicals under NIR-II laser and X-ray stimulation, and hydroxyl radicals initiate radical chain reactions to degrade methylene blue, resulting in a decrease in the absorbance of methylene blue [33]. The results showed that compared with the control group, the absorbance of methylene blue was decreased after single NIR/IR stimulation, while that of methylene blue was significantly decreased after combined stimulation, indicating the potential of GT on double sensitizers (Fig. S4A in Supporting information).

The main mechanism of cell damage caused by IR is the breaking of DNA double bonds. When DNA breaks, the γ-H_2AX factor will be formed at the fracture site to activate the DNA damage repair signaling [34]. The radiosensitization efficiency of RGDc-GT was investigated by immunofluorescence assay to detect the DNA damage caused by different nanoparticles under X-ray irradiation. As shown in Fig. S4B (Supporting information), compared with phosphate buffer saline (PBS) and PBS + IR groups, the fluorescence of γ-H_2AX in gold mineralized thermal sensitive liposomes (GT) + IR and RGT + IR groups was significantly enhanced, indicating that GT and RGT significantly increased the X-ray damage to cells. This may be due to the interaction between gold nanoparticles and X-ray photons used for radiotherapy and the generation of electrons, while the interaction between electrons and water molecules produces free radicals, resulting in the breaking of

DNA double bonds. The strongest fluorescence was exhibited in the RGT group which may be caused by the RGDc-mediated cell uptake increased the cellular uptake of nanoparticles and improved IR-induced DNA damage.

As shown in Figs. S4C and D (Supporting information), cellular uptake of different formulations all exhibited a time-dependent increase. After co-incubation with Lewis lung carcinoma (LLC) cells, both coumarin 6 (C6) loaded gold mineralized liposomes (GT-C6) and RGDc modified C6 loaded gold mineralized liposomes (RGT-C6) + NIR groups showed significantly increased cell uptake of nanoparticles ($P < 0.01$, $P < 0.001$) compared with the GT-C6 group, which might be due to the modification of RGDc was facilitate cell uptake of particles by active targeting. However, there was no significant difference in cellular uptake between RGT-C6 and RGT-C6 + NIR, suggesting that photothermal effects had little effect on the uptake of RGT.

As shown in Figs. S5A and B (Supporting information), GT and RGT had good biocompatibility. Combined with the NIR or IR irradiation, the GT exhibited concentration-depended cytotoxicity when the concentration of aurum (Au) was higher than 100 μg/mL. In addition, compared with NIR or IR monotherapy, the cell survival rate of the GT and RGT group treated with NIR and IR combination decreased to 28.16% and 24.83%, respectively, indicating that both GT and RGT could be working as photothermal sensitizer and IR sensitizer to induced cytotoxicity. Due to the increase of cell uptake mediated by the modification of nanoparticles RGDc, the cytotoxicity of RGT was stronger than that of GT at the same concentration [35].

Figs. S5C and D (Supporting information) showed the cytotoxicity of GEM combined with NIR on LLC cells when the concentration of Au was higher than 5 μg/mL, the toxicity of GT and RGT to LLC cells was both concentration-dependent under NIR-II light stimulation. After GEM loading, GTG and RGTG both exhibited concentration-depended cellular apoptosis, suggesting the PTT combined with chemotherapy maybe increase the therapeutic efficiency in LLC killing *in vitro*. Figs. S5E and F (Supporting information) showed a concentration-dependent reduction in cell viability in the range of GTG and RGTG concentrations from 5 μg/mL to 200 μg/mL. With the concentration of Au was 200 μg/mL, the mean cell viability of the combination therapy group was 8.37% and 4.78%, respectively, which was significantly lower than that of the GEM + NIR group (27.79% and 21.55%, $P < 0.01$) and the IR + NIR group (28.10% and 24.83%, $P < 0.01$), strongly proves the synergistic cell-killing effects. We then used the Compusyn software (Combosyn, Inc., Paramus, NJ) to evaluate the synergistic efficiency of combined therapy. The synergy index result was shown in Fig. S5G (Supporting information). The abscissa Fa indicates the inhibition rate. The combination index (CI) value represented the various synergistic types of combination therapy, which the value of 0.90–1.10 representing the simple superposition effect, 0.85–0.90 representing the low synergy effect, 0.7–0.85 representing the medium synergy effect, 0.3–0.7 represents the high synergy effect, and 0.1–0.3 represents strong synergy effect [36]. When the inhibition rate was low (<60%), RGTG had no synergistic effect on LLC cells. With the increase of RGTG concentration, the CI value gradually decreased, and the synergistic effect gradually strengthened. When the content of RGTG was 5 μg/mL, the synergy index was 0.39, indicating a high degree of synergy. These results were similar to those of cytotoxicity. Therefore, chemotherapy combined with hyperthermia and radiotherapy could significantly improve the synergistic effect of lung cancer cocktail therapy.

As an important component of the tumor microenvironment, cancer-associated fibroblasts (CAF) were highly heterogeneous and could promote tumor metastasis, interstitial remodeling, and immunosuppression. Mixed tumor spheres were constructed by mixing activated fibroblasts (NIH/3T3) and LLC to simulate the microenvironment of solid tumors and the tight connection between cells. As shown in Figs. 2A and B, free coumarin only stayed outside the sphere due to the tight connection of the tumor surface spheres. Compared with TSL-C6 and GT-C6 alone, the NIR irradiation combined GT-C6 signals was founded at the 40.3% depth of the tumor spheres, suggesting the NIR combined with GT could significantly improve the penetration of the particles in the solid core. This might be due to the GNPs can transform activated CAF into a quiescent state under the NIR irradiation. At the same time, the glucose around the tumor sphere also could be consumed, resulting in starvation therapy, which reduces the pH value and enhances the activity of nano enzymes and promotes the penetration of nanoparticles into the deep tumor [36]. After NIR and IR stimulation, the penetration depth of coumarin in the RGT-C6 group further increased to 59.7%. This might be attributed to the synergistic effects of CAF quiescent, cell starvation, and irradiation-induced cellular connection interruption, which allowed the nanoparticles penetrate to the deep layer of the tumor sphere.

The mixed tumor sphere model was also used to verify the effect of triple therapy *in vitro*. As shown in Figs. 2C and D, the

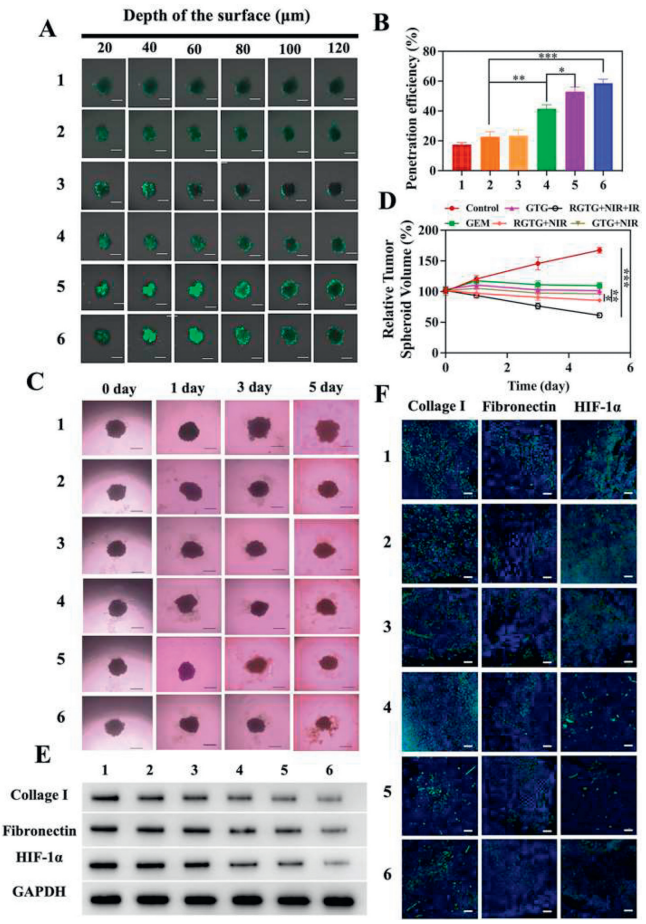

Fig. 2. (A) The confocal laser microscope of different C6 labeled formulations into LLC tumor spheroids to different depths for 6 h. Scale bar: 100 μm. 1: free C6; 2: TSL-C6; 3: GT-C6; 4: GT-C6 + NIR; 5: RGT-C6 + NIR; 6: RGT-C6 + NIR + IR. (B) Penetration efficiency of fluorescence of different preparations in mixture tumor spheroids. (C) Inhibition of LLC mixture tumor spheroid growth by GEM preparations at 5 μg/mL for 5 days. Scale bar: 100 μm. (D) Statistical results of the inhibition of tumor spheroid growth by GEM preparations at 5 μg/mL for 5 days. $^{*}P < 0.05$, $^{**}P < 0.01$, $^{***}P < 0.001$. (E) Western blot of the expression of related proteins in tumor globules after different treatment groups. (F) Representative immunofluorescence images of collage I, fibronectin, and HIF-1α expression after various therapeutic strategies. Scale bar: 200 μm. 1: PBS; 2: Free; 3: GTG; 4: GTG + NIR; 5: RGTG + NIR; 6: RGTG + NIR + IR. GAPDH: glyceraldehyde-3-phosphate dehydrogenase. Each bar represents the mean ± SD, n=3.

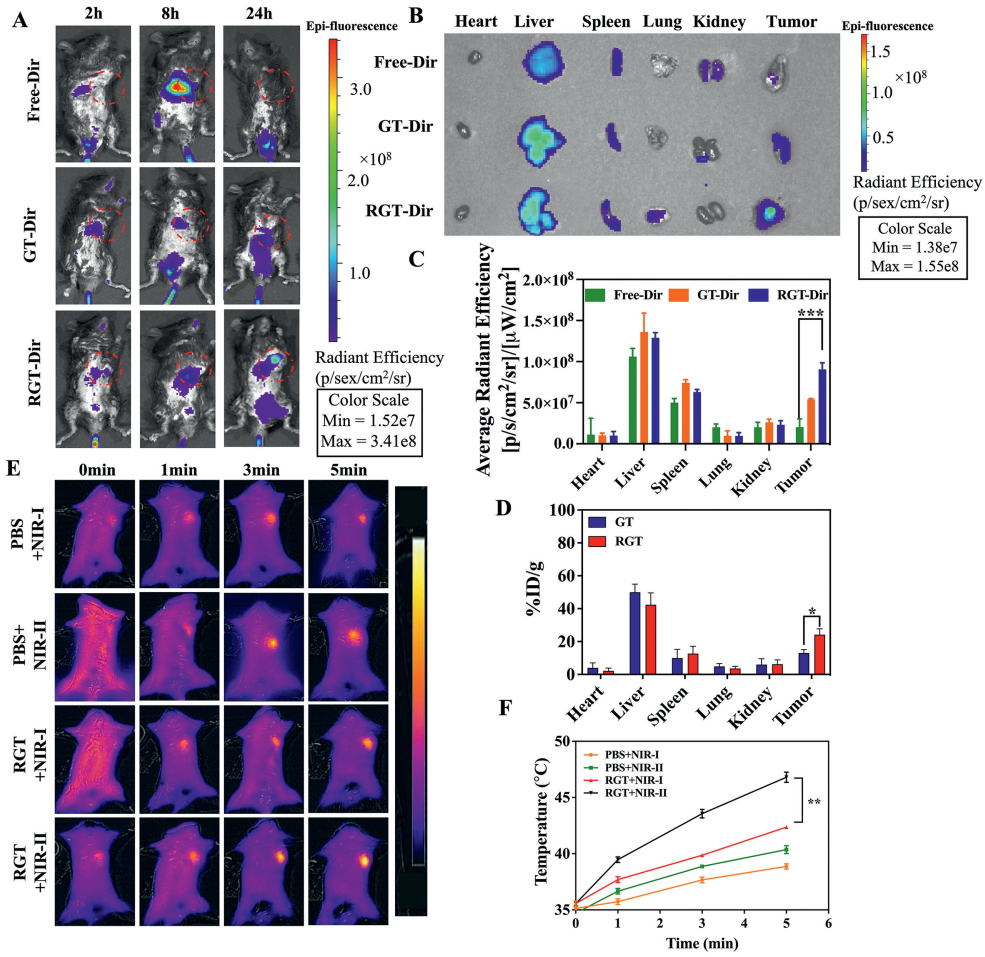

Fig. 3. (A) The *in vivo* imaging of LLC tumor mice after intravenous injection of free Dir, GT-Dir, and RGT-Dir. Red circles represent the tumor site. (B) The images of *ex vivo* organs of mice at 24 h after injection free Dir, GT-Dir, and RGT-Dir. (C) The average fluorescence intensity of *ex vivo* organs and tumors of mice at 24 h after injection of different groups ($n = 3$). (D) The average Au amount of *ex vivo* organs and tumors of mice at 24 h after injection of different groups ($n = 3$). (E) *In vivo* photothermal imaging with a NIR laser at 0, 1, 3 and 5 min of LLC tumor mice 24 h after intravenous injection of PBS and RGT. (F) Temperature changes of the LLC tumor mice during NIR-I and NIR-II irradiation at different points of different groups ($n = 3$). $^{*}P < 0.05$, $^{**}P < 0.01$, $^{***}P < 0.001$. %ID/g: the percentage injected dose per gram of tissue. Each bar represents the mean ± SD.

volume of untreated tumor spheres gradually increased. The tumor volume of the GEM group remained unchanged, suggesting GEM alone could partially inhibit tumor proliferation on the tumor surface but hardly penetrated the core of the tumor sphere. After chemotherapy combined with hyperthermia or radiotherapy, due to the good photo-thermal conversion effect and radiosensitization ability of gold nanoparticles, the tumor sphere volume decreased more significantly ($P < 0.01$). RGTG + NIR + IR group showed the most effective therapeutic effect. The sphere was loose and disintegrated on the fifth day, and the tumor volume decreased to 57.32% of the original tumor volume, which might be caused by the resting fibroblasts of gold nanoparticles and the improvement of tumor hypoxia by glucose oxidase [36]. Moreover, various proteins related to hypoxia and extracellular matrix were determined by western blot assay, including hypoxia-inducible factor 1α (HIF-1α), fibronectin, and collagen I. As shown in Fig. 2E, the expression of HIF-1α in GTG and RGTG groups was decreased, indicating that gold nanoenzyme could improve tumor hypoxia under the NIR irradiation. In addition, the decrease of fibronectin and collagen I content in the RGTG + NIR + IR group showed that heating and radiotherapy reduced the production of fibroin and collagen in tumor tissue. We further determined the expression of key proteins during triple therapy by the immunofluorescence assay. The lowest expression of collage I, fibronectin, and HIF-1α in GTG + NIR + IR and RGTG + NIR + IR groups, indicating that they could synergically relieve the hypoxic microenvironment and inhibit tumor proliferation ability (Fig. 2F).

In vivo targeting of different formulations has also been investigated. All animal studies were approved by the Animal Care and Use Committee of the China Pharmaceutical University (No. 2021–02–004). The results showed that free Dir injected into the body was mainly accumulated in the liver and rapidly eliminated within 24 h (Fig. 3A). The fluorescence of GT-Dir increased with the prolongation of administration time, and the fluorescence of tumor tissue was higher than that of free Dir group (Fig. 3B). This might be due to the EPR effect caused by the high permeability and retention effect of lipid particles due to the rich blood vessels in tumor tissue, the wide gap between blood vessels and the fast blood flow [37]. RGDc modification significantly improved the tumor tissue accumulation of Dir signal compared to the GT-Dir groups due to their active targeting ability. Moreover, fluorescence images of all organs at 24 h further showed the RGT-Dir group was 1.8 times that of the GT-Dir group, and 4.5 times that of the free Dir group, indicating that RGDc modification can enhance the tumor-targeting ability of the GT-Dir group (Fig. 3C). Compared to the unmodified GT group, the concentration of Au in the tumors of the RGDc-

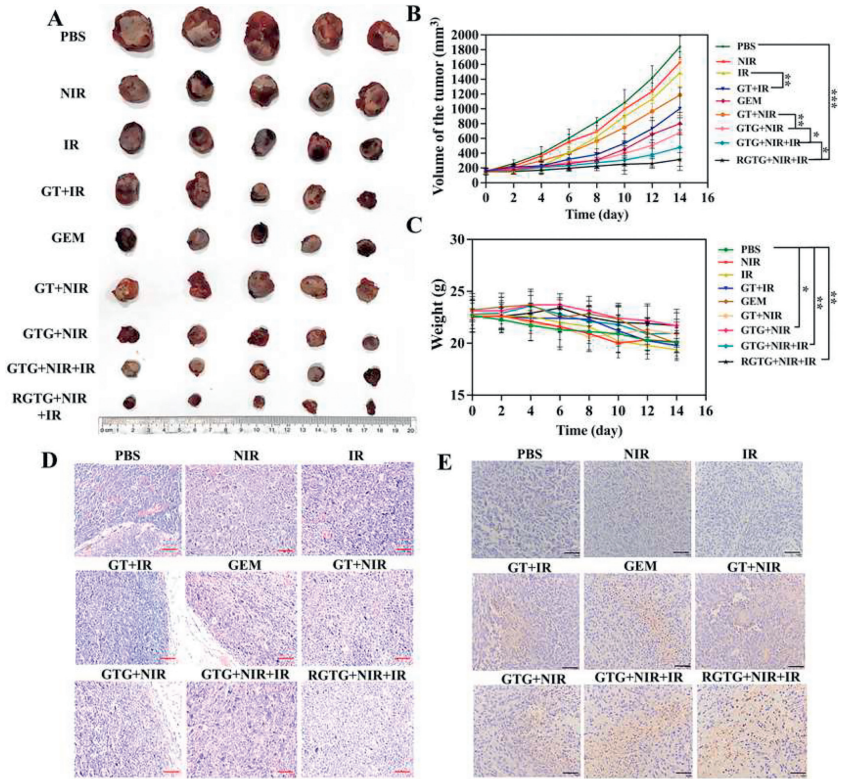

Fig. 4. (A) The tumor images of different treatment groups after 14-day treatment. (B) Tumor volume changes in different treatment groups within 14 days ($n = 5$). (C) The weight changes of mice in all at 14 days. (D) Representative H&E staining images of tumor tissues after different treatments. (E) Representative TUNEL staining images of tumor tissues after different treatments. Scale bar: 100 μm. mean ± SD. $^{*}P < 0.05$, $^{**}P < 0.01$, $^{***}P < 0.001$.

coated RGT group was 1.9 times higher than that of the GT group, indicating that RGDc modification can significantly increase drug accumulation in tumors (Fig. 3D).

The first NIR light window (NIR-I, 650–900 nm) is physically limited by penetrating tissue, resulting in the treatment of PTT being challenged by deep tumor tissue [38]. Compared with NIR-I, NIR-II provides better tissue penetration, lower background signal, higher safety limits, and photothermal conversion capabilities [39]. Fig. 3E showed the temperature changes of tumor sites in mice after laser irradiation in NIR-I and NIR-II regions after intravenous injection of RGDc-modified gold mineralized thermosensitive liposomes (RGT). The results showed that the temperature of the tumor site was significantly increased after injection of RGT in both NIR-I and NIR-II regions, indicating that RGT had a relatively good photothermal conversion effect *in vivo*. Compared with the NIR-I region, RGT heats up rapidly under light irradiation in the NIR-II region, reaching the temperature required for tumor treatment (42 °C) in about 1–2 min. This might be due to the better penetration of RGT in the NIR-II region compared to NIR-I. After 5 min, the temperature of the tumor site could be increased to about 46.3 °C, which was significantly higher than that of the NIR-I laser ($P < 0.01$) (Fig. 3F), suggesting that induce tumor cell apoptosis without damaging normal tissue. Therefore, RGT in response to the NIR-II region could help improve compliance with treatment and reduce the dosage required during treatment.

The tumor volume and body weight of mice in each group were recorded during the treatment (Figs. 4A–C). The results showed that tumors in the blank control group, NIR group, and IR group had not significantly reduced, suggesting the PTT and RT therapy alone hardly inhibited the tumor growth. For the mice in the GT + NIR group and GT + IR group, tumor size was reduced after the NIR or IR therapy, indicating the GT expressed as a dual sensitizer to improve the tumor cell apoptosis after irradiation. After combining with the GEM, the triple cocktail therapy strategy exhibited better tumor inhibition compared to monotherapy or dual therapy, confirming the advance of the multi-therapy on LLC treatment. After the RGDc modification, mice in the RGTG + NIR + IR group showed the lowest tumor size in all groups, with a tumor volume reduction of 83% compared to the control group, which benefited from the RGDc-based tumor targeting ability. RGDc modification allowed more nanoparticles located and accumulated in tumor tissue and released GNPs could induce fibroblasts resting under the stimulation of NIR-II, further increasing the penetration of RGTG. As an enzyme similar to peroxidase, GNPs consume glucose at tumor sites and cut off energy supply, leading to starvation treatment and enhancing the effect of radiotherapy [40]. In addition, in the blank control group, NIR group, RT group, and GEM group, mice body weight decreased rapidly due to the poor inhibition of tumor tissue proliferation (Fig. 4C). While that in other therapeutic groups were exhibited a slight decrease, indicating that there was no serious toxicity of RGT carriers and combination therapy could effectively inhibited tumor generation terminal deoxynucleotidyltransferase-mediated dUTP nick-end labeling (TUNEL) analysis has been used to evaluate cell apoptosis. The tissue section images showed that the tumors in the GEM group, GTG + NIR group, and GTG + NIR + IR group all expressed apoptosis features, and the tumor cells expressed necrosis and nuclear loss. Among them, RGTG + NIR + IR group had the strongest tumor cell apoptosis after treatment, suggesting that its killing effect was the most significant (Figs. 4D and E). To evaluate the biocompatibility and toxicity *in vivo*, the hematoxylin-eosin staining (H&E) staining of main organs from mice in all treatment groups was evaluated. As shown in Fig. S6 (in Supporting information), compared with the control group, no obvious pathological changes were observed in all treatment groups, suggesting the particles had good biocompatibility and would not induce the obvious inflammation.

The permeability of nanoparticles was also studied *in vivo* through the administration of Rhodamine B loaded preparation and evaluated using laser scanning confocal microscopy (LSCM) (Figs. S7 and S8 in Supporting information). It was suggested that RGTG was a promising nano preparation to promote drug penetration. In addition, RGTG could enhance drug permeability by reducing the expression of alpha smooth muscle actin (α-SMA), fibroblast activation protein (FAP), fatty acid synthase (FASN), and fibronectin, while CAFs quiescent (Fig. S9A–D in Supporting information). These results lay the foundation for the application of combination therapy in cancer treatment.

In summary, we designed an RGDc-modified gold mineralized lipid nanoparticle delivery platform, which has excellent *in vitro* and *in vivo* targeting efficacy for NSCLC and can be used for targeted drug delivery for NSCLC. The prepared RGTG released gold nanoparticles under the stimulation of NIR-II to induce CAFs quiescence, reshape ECM, and release GEM to inhibit cell proliferation. In addition, the released gold nanoparticles can produce starvation therapy by consuming glucose around tumor tissues, and improve the sensitivity of radiotherapy and hyperthermia, to achieve the synergistic therapeutic effect of starvation-NIR-II PTT-IR. This work provides a promising strategy for the synergistic treatment of tumors by modulating the metabolic pathways of tumor cells.

Declaration of competing interest

The authors declare that they have no known competing financial interests or personal relationships that could have appeared to influence the work reported in this paper.

Acknowledgment

This work was supported by the National Natural Science Foundation of China (No. 81972892).

Supplementary materials

Supplementary material associated with this article can be found, in the online version, at doi:10.1016/j.cclet.2023.109296.

References

[1] H. Sung, J. Ferlay, R.L. Siegel, et al., CA Cancer J. Clin. 71 (2021) 209–249.
[2] S.K. Alam, L. Wang, Z. Zhu, L.H. Hoeppner, NPJ Precis. Oncol. 7 (2023) 33.
[3] S. Garinet, P. Wang, A. Mansuet-Lupo, et al., Cancers 14 (2022) 1400.
[4] J. Vansteenkiste, E. Wauters, B. Reymen, et al., Annals Oncol. 30 (2019) 1244–1253.
[5] M. You, Z. Xie, N. Zhang, et al., Signal Transduc. Target. Ther. 8 (2023) 196.
[6] J. Li, D. Tong, J. Lin, J. Zhejiang Univ. 51 (2022) 241–250.
[7] X. Fan, Z. Luo, Y. Chen, et al., Acta Biomater. 142 (2022) 274–283.
[8] M. Wang, M. Chang, P. Zheng, et al., Adv. Sci. 9 (2022) e2202332.
[9] Y. Xu, S.Y. Liu, L. Zeng, et al., Adv. Mater. 34 (2022) e2204733.
[10] Z. Ding, D. Wang, W. Shi, et al., Int. J. Nanomed. 15 (2020) 8383–8400.
[11] L. Zhou, J. Jiang, Z. Huang, et al., Mol. Cancer 21 (2022) 168.
[12] W. Wang, X. Liu, X. Zheng, et al., Adv. Healthc. Mater. 9 (2020) e2001117.
[13] K. Kawasaki, A.V. Buchanan, K.M. Weiss, Ann. Rev. Genet. 43 (2009) 119–142.
[14] P. Srivastava, S.K. Hira, D.N. Srivastava, et al., ACS Appl. Mater. Interfaces 10 (2018) 6917–6929.
[15] S. Yao, B. Jin, Z. Liu, et al., Adv. Mater. 29 (2017) 1605903.
[16] S. Qing, C. Lyu, L. Zhu, et al., Adv. Mater. 32 (2020) e2002085.
[17] Z. Jiang, Y. Liu, R. Shi, et al., Adv. Mater. 34 (2022) e2110094.
[18] Y. Hu, H. Cheng, X. Zhao, et al., ACS Nano 11 (2017) 5558–5566.
[19] Z. Zhang, L.M. Bragg, M.R. Servos, J. Liu, Chin. Chem. Lett. 30 (2019) 1655–1658.
[20] L.H. Fu, C. Qi, J. Lin, P. Huang, Chem. Soc. Rev. 47 (2018) 6454–6472.
[21] H. Dai, Q. Fan, C. Wang, Exploration 2 (2022) 20210157.
[22] M. Zhao, R. Wang, K. Yang, et al., Acta Pharm. Sin. B 13 (2023) 916–941.
[23] H. Zhang, P. Xu, X. Zhang, et al., Chin. Chem. Lett. 31 (2020) 1083–1086.
[24] B. Chen, L. Mei, R. Fan, et al., Chin. Chem. Lett. 32 (2021) 1775–1779.
[25] P. Zheng, J. Ding, Asian J. Pharm. Sci. 17 (2022) 1–3.
[26] P. Zheng, B. Ding, R. Shi, et al., Adv. Mater. 33 (2021) e2007426.
[27] X. Xue, H. Qu, Y. Li, Exploration 2 (2022) 20210134.
[28] Y. Li, W. Song, Y. Hu, et al., J. Nanobiotechnol. 19 (2021) 293.
[29] W. Luo, C. Zhu, S. Su, et al., ACS Nano 4 (2010) 7451–7458.
[30] S. Wang, W. Chen, A.L. Liu, et al., ChemPhysChem 13 (2012) 1199–1204.
[31] B. Sampadi, S. Vermeulen, B. Mišovic, et al., Cells 11 (2022) 3794.
[32] A. Huwaidi, B. Kumari, G. Robert, et al., J. Phys. Chem. Lett. 12 (2021) 9947–9954.
[33] X.L. Cheng, T.R. Fu, D.F. Zhang, et al., Anal. Biochem. 667 (2023) 115087.
[34] L. Ronchetti, E. Melucci, F. De Nicola, et al., Int. J. Cancer 140 (2017) 2587–2595.
[35] Y. Yin, W.W. Zhu, L.P. Guo, et al., J. Phys. Chem. B 117 (2013) 125–131.
[36] Y. Liu, Z. Ye, W. Yang, et al., J. Control. Release 345 (2022) 120–137.
[37] Q. Zhou, J. Li, J. Xiang, et al., Adv. Drug Deliv. Rev. 189 (2022) 114480.
[38] Y. Zhang, S. Zhang, Z. Zhang, et al., Front. Chem. 9 (2021) 728066.
[39] S. Jiang, J. Lin, P. Huang, Adv. Healthc. Mater. 12 (2022) e2202208.
[40] C. Hu, M. Niestroj, D. Yuan, et al., Int. J. Nanomedicine 10 (2015) 2065–2077.